

Cite this article as: E Shun, Deng Jiacheng, Wang Henan, et al. Effect of Sc Addition on Corrosion Behavior of As-cast Al-3Cu-1Li Alloy in Acidic NaCl Solution[J]. Rare Metal Materials and Engineering, 2023, 52(06): 2048-2056.

ARTICLE

Effect of Sc Addition on Corrosion Behavior of As-cast Al-3Cu-1Li Alloy in Acidic NaCl Solution

E Shun¹, Deng Jiacheng², Wang Henan¹, Feng Changjie¹

¹ School of Materials and Engineering, Shenyang Aerospace University, Shenyang 110136, China; ² Xinyu Iron & Steel Group Co., Ltd, Xinyu 338001, China

Abstract: The effect of Sc addition on the corrosion behavior of as-cast Al-3Cu-1Li alloy in 2 mol/L NaCl acidic solution was studied. The phase compositions of as-cast Al-3Cu-1Li-xSc (mass fraction) alloys were determined by XRD. The microstructures of Al-3Cu-1Li alloy and Al-3Cu-1Li-0.5Sc alloy were observed by FE-SEM/EDS and TEM. The corrosion behavior of the alloy was studied by potentiodynamic polarization, EIS, EN and immersion test, and the corrosion mechanism was discussed. The results show that Cu-rich spherical phases are distributed in the grain of Al-Cu-1Li alloy; Cu-rich spherical phase is reduced, and W phase precipitates at the grain boundary of Al-3Cu-1Li alloys containing Sc. Sc can reduce the corrosion reaction activation energy of the alloys, making the corrosion process easier. With increasing the Sc content, cathode hydrogen evolution rate increases, the self-corrosion current density of the alloy increases, and the corrosion resistance decreases gradually. EN and EIS results show that the surfaces of Al-3Cu-1Li alloy and Al-3Cu-1Li-0.1Sc alloy are in the state of “film rupture-repassivation” during 12 h immersion in the solution, and Al-3Cu-1Li-0.3Sc alloy and Al-3Cu-1Li-0.5Sc alloy have severe intergranular corrosion.

Key words: Sc-containing Al-Cu-Li alloy; acidic NaCl solution; W phase; Cu-rich phase; electrochemical noise

Compared with traditional aluminum alloys, Al-Li alloys have lower density and higher elastic modulus (the density is decreased by 3% and the Young's modulus is increased by 6% at 1% lithium addition^[1]). Some relatively mature Al-Li alloy systems have been applied to aerospace and military equipment fields. For example, 2195 Al-Li alloy has replaced traditional aluminum alloy to manufacture rocket body structure, reducing the density by 5%, increasing the strength by 30%, and significantly improving the rocket's carrying capacity^[2]. Russia has developed a series of Al-Li alloys containing Sc, such as 1451, 1460, 1461 and 1464 Al-Li alloys^[3]. Al-Li alloys containing Sc have attracted wide attention due to their low density, high specific strength and specific stiffness, excellent weldability and corrosion resistance. Adding Sc into aluminum alloy can play a dual role of transition metal and rare earth element and effectively improve the microstructure. Due to the decrease in strain energy and surface energy of Al-Li alloy, Al₃Sc particles can be used as the nucleation core of Al₃Li, and finally transform into Al₃(Li, Sc) particles. Sc in Al-

Cu alloy can effectively promote the precipitation of Al₂Cu and the formation of Al₃Sc strengthening phase^[4-5]. Meanwhile, nanosized Al₃Sc particles in the alloy are not easy to be sheared by dislocation during plastic deformation, which can improve the toughness of aluminum alloy^[6]. In some Al-Cu-Li alloys such as 2099 and 1460 alloys, adding a small amount of Sc effectively refines the grain structure and inhibits the recrystallization^[7]. However, the addition of Sc in copper-rich aluminum alloy is easy to form a ternary W phase^[8], and it is considered as Al_{8-x}Cu_{4-x}Sc^[9], Al₅₋₈Cu₇₋₄Sc^[10] or Al_{5.4-8}Cu_{6.6-4}Sc^[11] compounds. The formation of a coarse W phase instead of Al₃Sc will reduce the positive effect of Sc and decrease the mechanical properties of the alloy.

There are a few reports on the corrosion behavior of Sc in aluminum alloy. Qiu^[12] found that adding Sc and Zr to AA5182 rolled sheet can reduce the corrosion depth and mass loss in 0.5 mol/L NaCl solution. Peng^[13] studied the effect of Sc on the corrosion resistance of 7050 aluminum alloy, and found that the addition of trace Sc improves the corrosion

Received date: November 23, 2022

Foundation item: Liaoning Revitalization Talents Program (XLYC 2002031)

Corresponding author: Wang Henan, Ph. D., Associate Professor, School of Materials and Engineering, Shenyang Aerospace University, Shenyang 110136, P. R. China, Tel: 0086-24-89724198, E-mail: wanghenan1@stu.sau.edu.cn

Copyright © 2023, Northwest Institute for Nonferrous Metal Research. Published by Science Press. All rights reserved.

resistance and reduces the intergranular corrosion, stress corrosion and exfoliation sensitivity of the alloy. Similarly, Liu^[14] added trace Sc to the 7050 alloy instead of Cu, and the self-corrosion potential and self-corrosion current density decrease. Kairy^[15] reported that the corrosion type of Al-Cu alloy changes from IGC to IGC+pitting after the addition of Sc. The effect of Sc content on the corrosion of Al-2Li-2Cu-0.5Mg-xSc alloy was studied^[16]. It is found that the alloy with 0.1wt% Sc has the best corrosion resistance in NaCl solution, and the corrosion resistance of solid solution alloy is better than that of as-cast alloy and aging alloy. Most studies focused on the passivation behavior of neutral NaCl or intergranular corrosion behavior in NaCl+H₂O₂ environment. The effect of Sc addition on the corrosion behavior of Al-Li alloy in acidic solution has rarely been studied. This study selected Al-3Cu-1Li alloy containing a small amount of Sc as the experimental material to investigate the corrosion behavior in acidic NaCl solution, and the corrosion mechanism was also discussed.

1 Experiment

High-purity aluminum (99.99%) and Al-50%Cu, Al-5%Li and Al-5%Sc alloys were used as raw materials, Al-3Cu-1Li-xSc alloys were prepared by the flux protection melting in a resistance furnace at 750 °C. The alloy was completely melted and stirred evenly, then poured into the graphite mold and cooled in air. The alloy composition was measured by inductively coupled plasma atomic absorption spectrometry (ICP-AES). The content of Sc was 0wt%, 0.09wt%, 0.25wt% and 0.46wt% in the alloys, marked as 0Sc, 0.1Sc, 0.3Sc, and 0.5Sc alloy, respectively.

After grinding with SiC paper (240#–2000#) and polishing, the samples were etched with Keller's reagent. The microstructures of Al-3Cu-1Li alloy and Al-3Cu-1Li-0.5Sc alloy were observed by FE-SEM/EDS and TEM. Phase analysis was performed by XRD.

Then 2 mol/L NaCl acid solution (pH=2) was used as the test solution. The pH value was adjusted by 0.5 mol/L H₂SO₄ solution, and the solution was prepared with an analytical reagent and distilled water. The temperature remains at 30±2 °C.

The electrochemical test was carried out using an electrochemical workstation (Autolab PGSTAT302N). The standard three-electrode system includes platinum plate as the counter electrode, saturated calomel electrode (SCE) as the reference electrode, and the sample as the working electrode. After immersion in solution for 1800 s, the potentiodynamic polarization curve was measured from 250 mV below the self-corrosion potential, and scanning rate was 20 mV/min. The corrosion current density i_{corr} at different temperatures

(30–50 °C) was measured by the linear polarization, and the molar activation energy E_a was calculated by the Arrhenius formula^[17]:

$$\log i_{\text{corr}} = \log A - \frac{E_a}{20303RT} \quad (1)$$

where A is a pre-factor; R is a gas constant (8.314 J·mol⁻¹·K⁻¹); T is the absolute temperature. Electrochemical impedance used 10 mV sinusoidal perturbation in the frequency range of 10⁵ Hz–0.01 Hz, and 50 points were taken. The above electrochemical measurement was repeated three times.

The electrochemical noise (EN) of the alloy in the test solution was measured by the electrochemical noise module. Two identical samples were used as working electrode 1 and 2. The reference electrode was a saturated calomel electrode. Each noise data set was 1024 s, with 0.25 s in sampling interval, and 12 h in recording time. The fifth-order polynomial fitting method was used to eliminate the DC drift of the original data^[18].

Polished 0.1Sc alloy and 0.5Sc alloy were immersed in the test solution for 16 d, with a surface volume ratio of 1:50 (cm²/mL). According to GBT16545-1996, the corrosion products of the alloys were removed by immersing in concentrated nitric acid for 5 min at room temperature. The corrosion morphology was observed by SEM.

2 Results and Discussion

2.1 Phase composition and microstructure of as-cast alloys

The XRD patterns of as-cast Al-3Cu-1Li-xSc alloy are shown in Fig.1. There are α -Al, Al₂Cu, AlCu and Al₄Li₃ phases in 0Sc alloy. W (AlCuSc) and T₂ (Al₇Cu₄Li) phases appear in three alloys containing Sc, and no Al₃Sc phase is found. Yang^[8] and Chen^[19] studied Al-2.5Cu-0.3Sc alloy, and no W phase forms. It has also been reported that there is no W phase in 2618 (Al-2.23Cu-1.21Mg-X) alloy with 0.3% Sc and 0.3% Zr^[20]. The W phase in Al-Cu-Mg-Ag alloy has a high Cu content (4.5%–5.6%), but no Al₃Sc particles form^[21–22]. The main strengthening phases of Al-Cu-Li alloy are T₁ (Al₂CuLi) and Al₂Cu. The formation of coarse W phase consumes a large amount of Cu and Sc atoms in the alloy, so the adding of Sc may lead to a significant decrease in strength and ductility. Jia^[11] also reported that coarse W phase forms after homogenization in 1469 (Al-4.2Cu-1Li-X) alloy. At present, the formation mechanism of W phase in Al-Cu-X-Sc alloys is unclear, and it is reported that W phase tends to form in Al alloy with relatively high Cu content (>3%)^[11,21–22]. Gong^[23] showed that when Cu content is reduced to less than 3%, that is, $w(\text{Cu})/w(\text{Sc})$ is less than 32, W phase will not form. Some researchers believe that the absolute Sc content or Cu/Sc ratio is not the only key factor for forming W phase. Additionally, it is found that some diffraction peaks in Sc-containing alloys are consistent with the characteristic peaks related to T_B (Al_{7.5}Cu₄Li). The results of Fridlyander^[24] show that T₁, Al₂Cu, AlLi, Al₂CuMg, Al₂MgLi, T₂ (Al₆CuLi₃) and T_B(Al_{7.5}Cu₄Li) phases coexist with the α -Al solid solution in Al-Li-Cu-Mg alloys. W phase can be formed in the Al-3Cu-1Li-xSc (x=0.1, 0.3, 0.5) alloys.

Table 1 Chemical composition of Al-3Cu-1Li-xSc alloy (wt%)

Alloy	Cu	Li	Sc	Al
Al-3Cu-1Li	3.17	0.86	-	Bal.
Al-3Cu-1Li-0.1Sc	3.03	1.09	0.09	Bal.
Al-3Cu-1Li-0.3Sc	3.07	0.82	0.25	Bal.
Al-3Cu-1Li-0.5Sc	3.15	1.10	0.46	Bal.

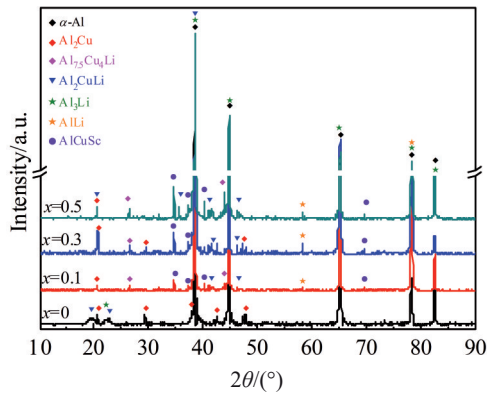


Fig.1 XRD patterns of as-cast Al-3Cu-1Li-xSc alloy

Previous studies showed that the average grain size of Al-3Cu-1Li alloy gradually decreases with increasing Sc content. The microstructure of 0Sc alloy and 0.5Sc alloy was observed by SEM backscatter electron and EDS analysis. The results are shown in Fig.2. Spherical particles (Fig.2a) with different sizes are uniformly distributed in the grain of 0Sc alloy, and semi-continuous precipitates (Fig. 2b) are precipitated at the grain boundary. EDS analysis shows that particle 1 is composed of Al and Cu elements (Fig.2c), and atomic ratio of Al/Cu is approximately equal to 1, which is the spherical Cu-rich phase. The atomic ratio of Al/Cu of precipitates at grain boundaries is about 2 (Fig. 2d), which should be the Al_2Cu phase. In the 0.5Sc alloy, the spherical Cu-rich phase in the grain decreases significantly, and Al_2Cu phase at the grain boundary increases. EDS analysis shows that the phases distributed along grain boundaries are composed of Al, Cu

and Sc. Cu is enriched in the second phase and distributed along grain boundaries, mainly composed of Al_2Cu and W phases. Sc element is evenly distributed. Table 2 shows the EDS results of the as-cast Al-3Cu-1Li-xSc alloy in the α -Al matrix. Due to the precipitation of Cu-rich spherical phase (AlCu) in 0Sc alloy, Cu content in the α -Al matrix is only 1.5wt%, and the solubility of Cu in Sc-containing alloys increases obviously.

The high-angle annular dark field image (HAADF) and EDS analyses of 0Sc alloy and 0.5Sc alloy are shown in Fig.3. In Fig.3a, it can be found that there is a brighter particle in the upper left, which has the element with higher atomic number. EDS analysis (Fig. 3c) determines that the particle is composed of Al and Cu. This spherical and micron-sized particle is the AlCu phase in 0Sc alloy. In the HAADF image of 0.5Sc alloy (Fig. 3b), bright spherical particles with a size of about 20 nm can be observed. EDS analysis (Fig. 3d) determines that the bright particles should be Al_2Cu phase. Some dark spherical particles with 10 nm in diameter are also distributed in the grain of 0.5Sc alloy. Combined with the SAED pattern (Fig. 3b) and XRD analysis, it can be determined that the dark particles are Al_4Li_9 phase. In addition, a slim needle-like T_2 phase precipitates in 0.5Sc alloy (Fig.3e).

2.2 Potentiodynamic polarization curve

Fig.4 shows the potentiodynamic polarization curves of as-cast Al-3Cu-1Li-xSc alloy in acidic 2 mol/L NaCl aqueous solution. It can be seen that the polarization curves of the alloys show similar behavior. With the increase in anodic potential, the current density increases gradually, and active dissolution occurs in the alloy. With the increase in Sc content, the cathodic hydrogen evolution curve shifts in the right

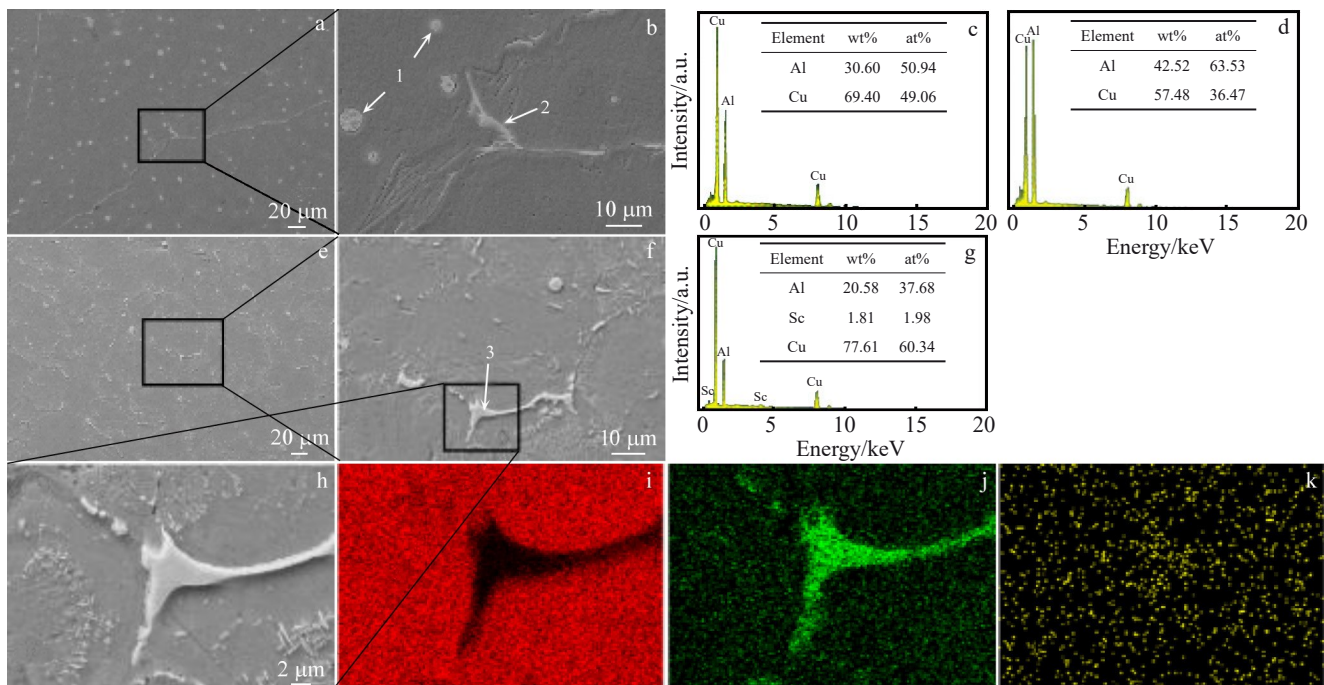


Fig.2 SEM back scattering electron images of 0Sc alloy (a, b) and 0.5Sc alloy (e, f, h); EDS results of particle 1 (c), grain boundary 2 (d) and grain boundary 3 (g); EDS mapping of element Al (i), Cu (j), and Sc (k) of 0.5Sc alloy

Table 2 EDS results of α -Al matrix of as-cast Al-3Cu-1Li-xSc alloys (wt%)

Element	0Sc	0.1Sc	0.3Sc	0.5Sc
Al	98.50	96.40	96.89	96.72
Cu	1.50	3.60	3.11	3.28

direction. The precipitation of Cu-rich cathode phase at grain boundaries in Sc-containing alloys increases, increasing the cathode reaction area and accelerating the hydrogen evolution rate. Table 3 shows the electrochemical parameters obtained by polarization curve fitting. With the increase in Sc content, the alloy's self-corrosion potential (E_{corr}) increases, and the

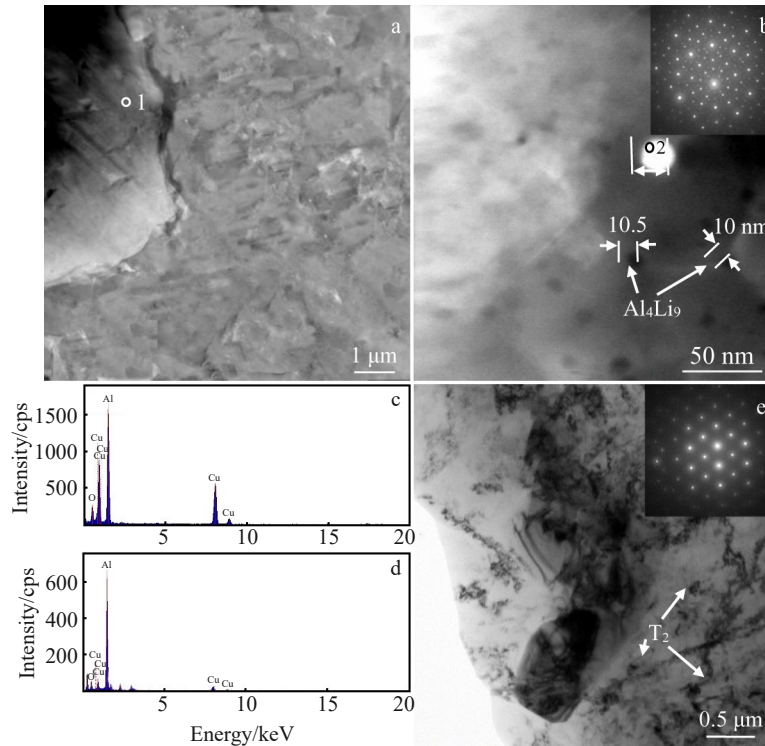


Fig.3 HAADF image of 0Sc alloy (a); HAADF image of 0.5Sc alloy and SAED pattern of Al_4Li_9 (b); EDS analysis of point 1 (c) marked in Fig.3a and point 2 (d) marked in Fig.3b; HAADF image and SAED patten of T_2 phase in 0.5Sc alloy (e)

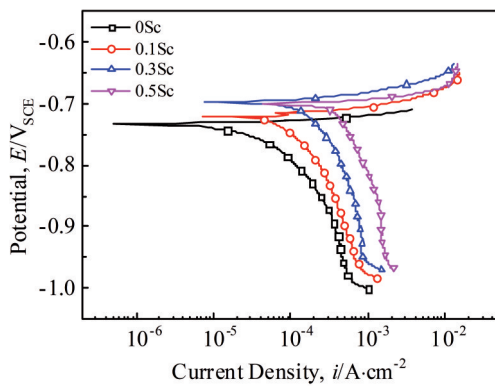


Fig.4 Potentiodynamic polarization curves of as-cast Al-3Cu-1Li-xSc alloy in acidic 2 mol/L NaCl aqueous solution (pH=2)

self-corrosion current density (i_{corr}) increases. According to Faraday's law^[25], the corrosion current density of the alloy is proportional to its corrosion rate, so Sc addition accelerates the corrosion rate of as-cast Al-3Cu-1Li-xSc alloy.

There is a relationship between the molar activation energy (E_a) of the chemical reaction and the corrosion resistance of the alloy^[26]. Usually, higher E_a indicates that corrosion

reaction is relatively difficult to occur, the alloy has high corrosion resistance. The linear polarization curves of the alloy at different temperatures were measured, and the self-corrosion current density was obtained by fitting, as shown in Fig.5a. The corrosion reaction E_a of the alloy was calculated according to the Arrhenius formula, and the results are shown in Fig.5b. It can be seen that the activation energy E_a of the alloy decreases with the increase in Sc content, making the corrosion reaction easier and decreasing the corrosion resistance.

2.3 Electrochemical impedance spectroscopy (EIS)

Electrochemical impedance spectroscopy is usually used to

Table 3 Fitted electrochemical parameters of polarization curves of as-cast Al-3Cu-1Li-xSc alloy

Alloy	$b_a/\text{V}\cdot\text{dec}^{-1}$	$b_c/\text{V}\cdot\text{dec}^{-1}$	$E_{\text{corr}}/\text{V}_{\text{SCE}}$	$i_{\text{corr}}/\mu\text{A}\cdot\text{cm}^{-2}$	R_p/Ω	$B/\text{mV}\cdot\text{dec}^{-1}$
0Sc	0.010	0.197	-0.734	56.26	232.4	4.216
0.1Sc	0.021	0.312	-0.721	139.48	184.5	8.684
0.3Sc	0.025	0.333	-0.698	223.06	114.99	10.257
0.5Sc	0.031	0.292	-0.700	405.12	67.89	12.207

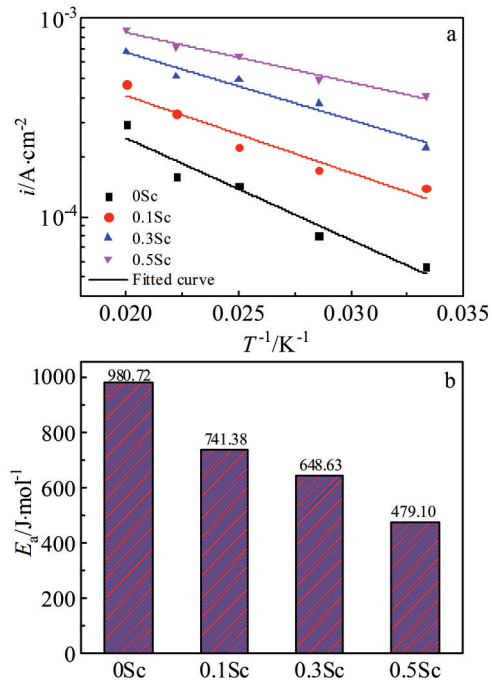


Fig.5 Self-corrosion current density (a) and molar activation energy (b) of the corrosion of as-cast Al-3Cu-1Li-xSc alloy

analyze the electrochemical corrosion mechanism of aluminum alloy. Fig.6 shows EIS measurement results of the as-cast Al-3Cu-1Li-xSc alloy. The Nyquist diagrams of 0Sc, 0.1Sc and 0.3Sc alloys consist of two arcs: a capacitive arc in the high-frequency region and an inductive arc in the low-frequency region; EIS of 0.5Sc alloy contains only one capacitive arc, and no inductive arc is found in the low-frequency region. The capacitive arc is related to the charge transfer process of electrical double layer between aluminum

alloy and the solution^[27]. The low-frequency inductive arc may be related to the weakening of the protective effect of the naturally formed oxide film caused by the active dissolution of aluminum alloy^[28]. Shi^[29] reported that the inductive arc of Al-Zn-Mg-Cu alloy and Al-Zn-Mg-Cu-Sc-Zr alloy disappears after immersion for 48 h, which is related to the dissolution of the oxide film and the corrosion of the exposed new surface. The disappearance of the inductive arc of 0.5Sc alloy may be the same as this result. Fig.6b shows the Bode diagrams of the four alloys. In the relationship curve of the phase angle and frequency, there are peaks representing capacitance and inductance^[30]. It can be seen that the peak of the capacitive arc of the four alloys is not symmetric, which is composed of two-time constants. One is associated with the surface film, and the other is related to the corrosion surface.

The equivalent circuit is used to further explain the corrosion behavior of the alloy, as shown in Fig. 6c (data fitting does not consider the data of inductive arc). The circuit elements can be defined as follows: R_s represents the solution resistance, R_p represents the resistance of corrosion area of the alloy surface, CPE_b is the equivalent capacitance of corrosion area, R_b and CPE_b are the resistance and capacitance of the alloy oxide film, respectively. Fig.6a shows the Nyquist plots of the experimental results (points) and fitting results (lines). The electrochemical impedance parameters of the equivalent circuit are listed in Table 4. It can be seen that with the increase in Sc content, R_b value of the alloy oxide film gradually decreases from 288.1 $\Omega \cdot \text{cm}^2$ to 40.53 $\Omega \cdot \text{cm}^2$. Due to the presence of corrosion products, R_p increases from 2.475 $\Omega \cdot \text{cm}^2$ to 19.89 $\Omega \cdot \text{cm}^2$, the value of $R_b + R_p$ decreases, and the corrosion resistance of the alloy decreases.

2.4 Electrochemical noise

Fig. 7 shows the time-domain spectrum fragment of current noise of as-cast Al-3Cu-1Li-xSc alloy. It can be seen that the

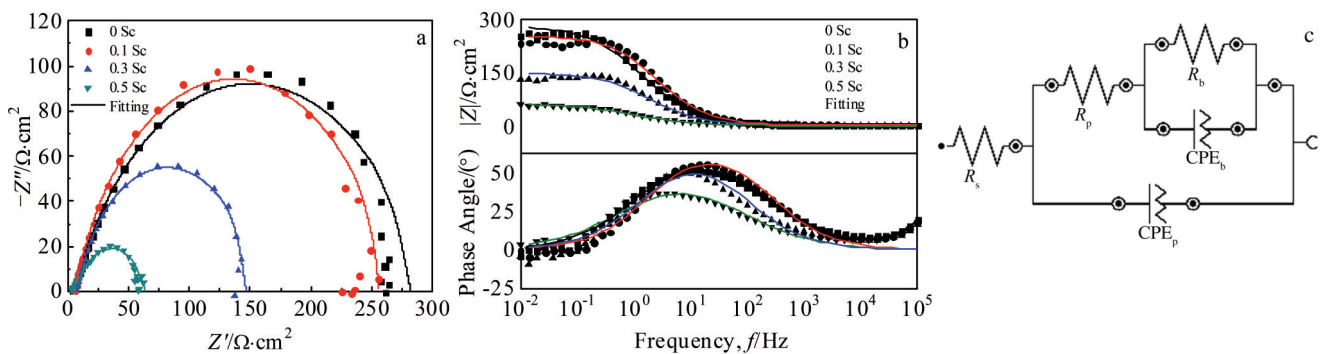


Fig.6 Nyquist curves (a), Bode diagram (b), and equivalent circuit (c) of as-cast Al-3Cu-1Li-xSc alloy after immersion for 4 h in test solution

Table 4 Impedance parameters of equivalent circuit obtained by fitting the experimental results of EIS

Alloy	$R_s/\Omega \cdot \text{cm}^2$	$C_p/\times 10^{-4} \text{F} \cdot \text{cm}^{-2}$	n_p	$R_p/\Omega \cdot \text{cm}^2$	$C_b/\times 10^{-4} \text{F} \cdot \text{cm}^{-2}$	n_b	$R_b/\Omega \cdot \text{cm}^2$
0Sc	4.105	2.720	0.744	2.475	7.599	0.718	288.1
0.1Sc	4.257	3.553	0.809	8.198	3.164	0.802	226.6
0.3Sc	5.811	5.245	0.854	9.236	8.109	0.801	140.2
0.5Sc	3.980	40.74	0.692	19.89	26.32	0.870	40.53

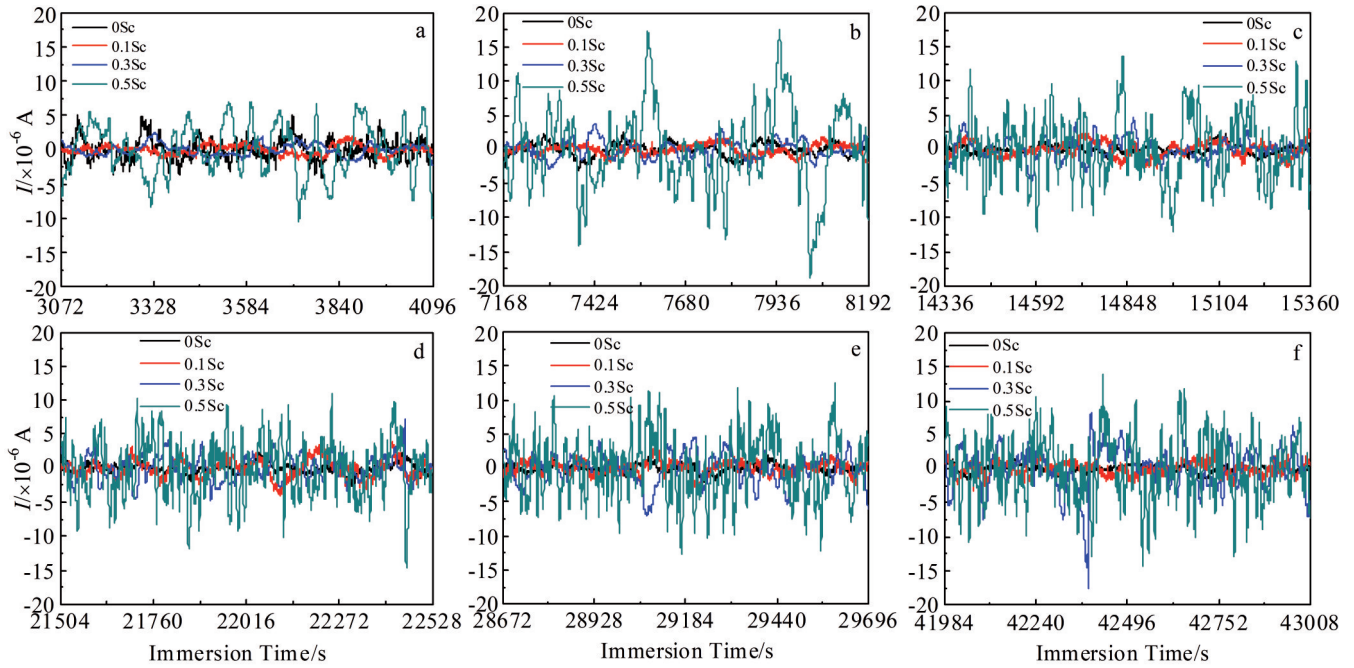


Fig.7 Time-domain spectrum fragment after DC trend removal of as-cast Al-3Cu-1Li-xSc alloy: (a) 3072–4096 s, (b) 7168–8192 s, (c) 14 336–15 360 s, (d) 21 504–22 528 s, (e) 28 872–29 696s, and (f) 41 984–43 008 s

current noise data fluctuates near zero after DC drift elimination. In initial immersion stage (Fig. 7a), the current intensity of 0Sc alloy is large, which indicate that the surface state of the alloy may not reach equilibrium. Other alloys have reached equilibrium before initial immersion stage. In later stages (Fig. 7b–Fig. 7f), the amplitude of the current noise vibration increases with the increase in Sc content. Within 12 h, the current noise signals of 0Sc and 0.1Sc alloys are in a typical transient peak state (small amplitude and high fluctuation frequency). Some researchers believe that this transient peak is due to the rapid alternating “film rupture-repassivation” process of the metal surface^[31]. With extension of immersion time, obvious characteristic peaks (large amplitude and small fluctuation frequency) appear in the time-domain spectrum of the current noise of 0.3Sc alloy, and the amplitude gradually increases (as shown in Fig. 7b–Fig. 7f). The appearance of characteristic peaks with an obvious increase in current intensity represents the corrosion of the alloy. The above characteristic peaks of 0.5Sc alloy appear at early stage of immersion; the amplitude increases from 5×10^{-6} A to 1.5×10^{-5} A and stabilizes at 1×10^{-5} A in the later stage. The corrosion process of the alloy can be judged by the fluctuation of the noise signal and the change of vibration amplitude. 0Sc and 0.1Sc alloys have no serious corrosion during the test process, and 0Sc alloy has the minimum current intensity; pit appears in 0.3Sc alloy after immersion for 2 h, then it enters the stage of pitting development and the quantity of pitting increases. 0.5Sc alloy has serious corrosion after immersion for 1 h.

Noise resistance is one of the most commonly used parameter for time-domain spectrum analysis of electrochemical noise, which can be calculated according to Eq.(2):

$$R_n = \frac{S_E}{S_I} \quad (2)$$

where R_n is noise resistance, and S_E and S_I are the standard deviations of potential noise and current noise, respectively.

The variation of alloy noise resistance with immersion time is shown in Fig. 8, which is inversely proportional to the instantaneous corrosion rate. During immersion, the noise resistance of 0.5Sc alloy is the smallest, 0.3Sc alloy is the second, 0.1Sc alloy and 0Sc alloy are relatively larger. When the test time is 14 400 s, the noise resistance R_n of 0Sc, 0.1Sc, 0.3Sc, and 0.5Sc alloys is 254, 227, 128, and 60 $\Omega \cdot \text{cm}^2$. The higher the Sc content of the alloy, the smaller the noise resistance and the greater the corrosion rate. The large abnormal value of the noise resistance of the alloy at the initial stage is because the electrode process has not yet reached the equilibrium state when it was put in the solution. During immersion, both 0Sc alloy and 0.1Sc alloy exhibit

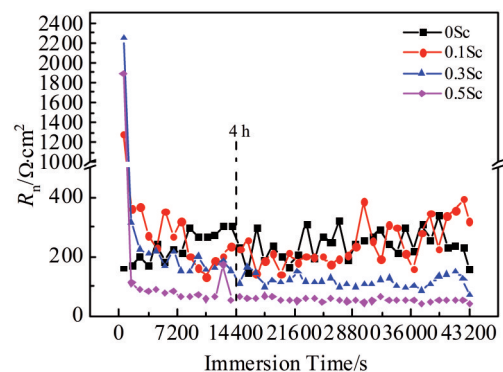


Fig.8 Variation of noise resistance of as-cast Al-3Cu-1Li-xSc alloy in the test solution

large noise resistance and amplitude fluctuations, indicating that the metal surface undergoes a competitive process of the surface film rupture and repassivation^[32]. In contrast, 0.3Sc alloy and 0.5Sc alloy show smaller noise resistance and amplitude fluctuations, which means that the repassivation process is hindered, and the alloy corrosion is aggravated. The noise resistance R_n is comparable to the polarization resistance R_p ^[33]. By comparing the noise resistance R_n and polarization resistance R_p (Table 3), it can be found that they have the same trend and similar values.

Fast Fourier transform (FFT) was performed on the current noise in different periods of Fig.7 to obtain the power spectral density (PSD) curve. Fig. 9 shows the PSD curve and the results after smoothing of as-cast Al-3Cu-1Li-xSc alloy immersed in the test solution at different time. Table 5 gives the frequency domain characteristic value of the current noise signal. W_L is the low-frequency white noise level, k is the high-frequency band slope, and f_c is the turning frequency (the intersection of the low-frequency white noise level and high-frequency band). The white noise-level W_L of the current noise can reflect the corrosion resistance of alloys, and the larger the W_L , the worse the corrosion resistance^[34]. The slope k can be used to judge the corrosion behavior of alloys^[31]. k value is close to -2 during this period, the surface of the sample is in the corrosion process of “film rupture-passivation”; the k value is close to -4 , indicating that the current noise signal is no longer generated instantaneously but slowly forms the current peak in linear or exponential form, and then exponentially decays along with time. At this time, pitting occurs on the alloy surface. 0Sc alloy and 0.1Sc alloy have smaller W_L values, and k value fluctuates around -2 ; W_L and k values of 0.3Sc alloys increase with the extension of

immersing time; the W_L value and k value of 0.5Sc alloys are the largest at the same period and the k value between -3.30 and -3.78 . With the increase in Sc content, the balance of “film rupture-repassivation” on the alloy surface is broken, the metal is exposed to the corrosion solution, and the current signal increases. As corrosion process progress, the formation of new corrosion products further hinders the corrosion process, resulting in the reduction of the current signal.

2.5 Immersion corrosion experiment

Fig. 10 shows the SEM images of as-cast 0Sc alloy (Fig.10a) and 0.5Sc alloy (Fig.10b) after immersion in the test solution for 16 d and the corrosion products have been removed. It can be seen that 0Sc alloy has many pits in the grain and slight intergranular corrosion. The 0.5Sc alloy has serious intergranular corrosion. The corrosion morphology is changed. Generally, the distribution and composition of precipitates directly affect the corrosion morphology of the alloy^[35]: Li is an active element, so the corrosion potential of the precipitates containing Li is negative, which is prone to corrosion; in contrast, the corrosion potential of Cu element is positive, and Cu-rich phase acts as a cathode in the corrosion microcells. Therefore, the α -Al matrix and grain boundary in contact with the Cu-rich phase are preferentially corroded. Pits in the grain of 0Sc alloy are formed by the detachment of spherical particles due to the corrosion of the α -Al matrix around Cu-rich spherical particles, and the corrosion also occurs around the second phase of the Cu-rich phase at the grain boundary. In 0.5Sc alloy, the spherical phase disappears and the corrosion occurs mainly at the grain boundary. From the microstructure of the alloy, Sc causes the Cu-rich spherical particles inside the grain to transform into the Al_2Cu phase at the grain boundary. The number of second phases at the grain

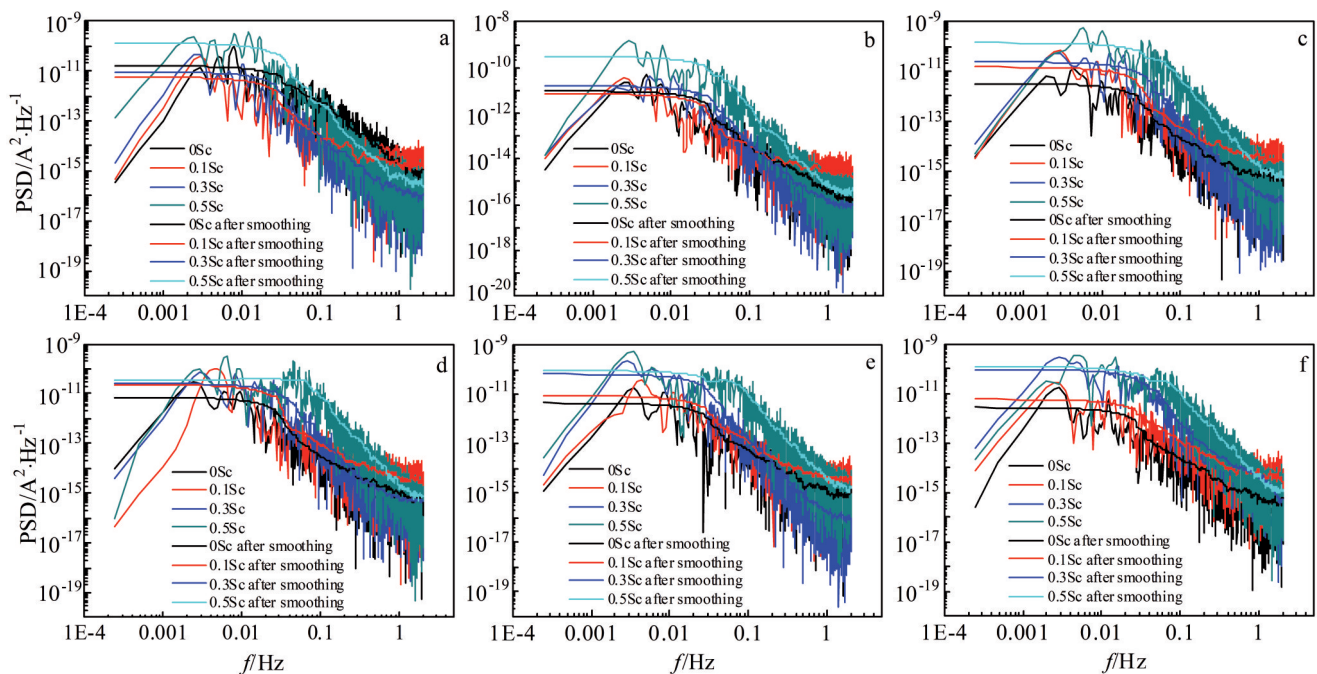


Fig.9 Current noise PSD of as-cast Al-3Cu-1Li-xSc alloy in test solution (corresponding to the time period of Fig.7): (a) 3072–4096 s, (b) 7168–8192 s, (c) 14 336–15 360 s, (d) 21 504–22 528 s, (e) 28 872–29 696s, and (f) 41 984–43 008 s

Table 5 Characteristic parameters from current noise PSD of as-cast Al-3Cu-1Li-xSc alloy in test solution

Parameter	Alloy	Fig.9a	Fig.9b	Fig.9c	Fig.9d	Fig.9e	Fig.9f
$W_L / \times 10^{-12} \text{ A}^2 \cdot \text{Hz}^{-1}$	0Sc	16.12	8.745	3.235	6.728	4.622	2.640
	0.1Sc	5.818	7.132	15.09	22.73	9.179	5.598
	0.3Sc	8.513	16.72	24.01	27.17	70.42	99.44
	0.5Sc	127.1	299.2	132.6	39.98	97.17	125.1
$k/\lg(\text{PSD})/10$	0Sc	-2.240	-2.167	-2.159	-2.340	-1.938	-1.896
	0.1Sc	-1.836	-1.886	-2.023	-2.011	-2.040	-1.790
	0.3Sc	-2.542	-3.172	-3.588	-3.301	-3.417	-2.957
	0.5Sc	-3.302	-3.686	-3.772	-3.615	-3.517	-3.331
f_c/Hz	0Sc	0.019	0.0086	0.010	0.011	0.0099	0.0087
	0.1Sc	0.0056	0.0060	0.011	0.0067	0.012	0.013
	0.3Sc	0.010	0.017	0.022	0.023	0.018	0.020
	0.5Sc	0.018	0.024	0.041	0.063	0.050	0.046

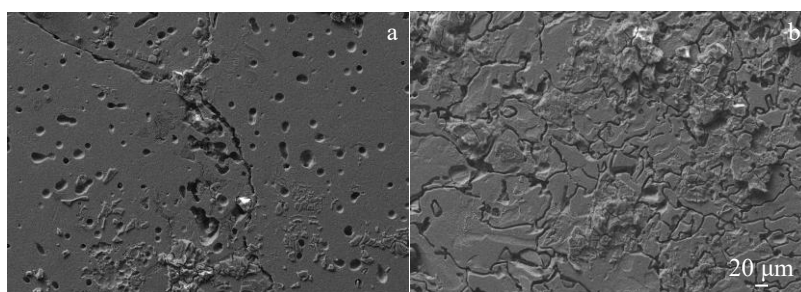


Fig.10 SEM micrographs of as-cast 0Sc (a) and 0.5Sc (b) alloy after immersion in the test solution for 16 d

boundary increases and the α -Al contacting with them preferentially dissolves, resulting in serious intergranular corrosion in 0.5Sc alloy.

3 Conclusions

1) The W phase in the Al-3Cu-1Li alloy containing Sc is precipitated at the grain boundary, and no Al_3Sc phase is found.

2) In 2 mol/L NaCl acidic solution (pH=2), anodic behavior of four alloys is active dissolution process, and Sc reduces the activation energy of the alloy reaction; Sc can accelerate the cathodic hydrogen evolution rate of the alloy, increase the self-corrosion current density and decrease the corrosion resistance of the alloy.

3) With the increase in Sc content, the active dissolution of aluminum alloy reduces the protective effect of the surface film, and the low-frequency inductive arc gradually disappears; the corrosion resistance of the alloy gradually decreases.

4) The Al-3Cu-1Li alloy and Al-3Cu-1Li-0.1Sc alloy are in the state of “film rupture-repassivation” and have pits in the grain and slight intergranular corrosion. Al-3Cu-1Li-0.3Sc alloy and Al-3Cu-1Li-0.5Sc alloy have serious intergranular corrosion. The immersion test supports this conclusion.

References

- Xie B X, Huang L, Xu J H et al. *Materials Science and Engineering A*[J], 2022, 832: 142-394
- Rioja R J, Liu J. *Metallurgical and Materials Transactions A*[J], 2012, 43(9): 3325
- Kolobnev N I. *Metal Science Heat Treatment*[J], 2002, 44(7-8): 297
- Cui J Z, Wang Z, Wang C X et al. *Rare Metal Materials and Engineering*[J], 2022, 51(5): 1724 (in Chinese)
- Feng L, Li J G, Mao Y Z et al. *Rare Metal Materials and Engineering*[J], 2019, 48(9): 2841 (in Chinese)
- Dai X Y, Xia C Q, Long C G et al. *Rare Metal Materials and Engineering*[J], 2011, 40(2): 265 (in Chinese)
- Ma J, Yan D S, Rong L J et al. *Progress in Natural Science: Materials International*[J], 2014, 24(1): 138
- Yang C, Zhang P, Shao D et al. *Acta Materialia*[J], 2016, 119: 68
- Norman A F, Prangnell P B, McEwen R S. *Acta Materialia*[J], 1998, 46(16): 5715
- Kharakterova M L, Eskin D G, Toropova L S. *Acta Metallurgica et Materialia*[J], 1994, 42(7): 2285
- Jia M, Zheng Z Q, Gong Z. *Journal of Alloys and Compounds*[J], 2014, 614: 131

- 12 Qiu Y C, Yang X F, Li J X et al. *Corrosion Science*[J], 2022, 199: 110-181
- 13 Peng H L, Ming X W, Qiao N G et al. *Light Alloy Fabrication Technology*[J], 2017, 45(7): 7 (in Chinese)
- 14 Liu D, Sang F, Li J et al. *Materials Characterization*[J], 2019, 158: 109-981
- 15 Kairy S K, Rouxel B, Dumbre J et al. *Corrosion Science*[J], 2019, 158: 108-095
- 16 Fang Q. *Effect of Trace Sc and Heat Treatment on Corrosion Resistance of Cast Al-Li-Cu Alloy*[D]. Shanghai: Shanghai Jiao Tong University, 2020 (in Chinese)
- 17 Wang L Q, Gao Z M, Liu Y J et al. *International Journal of Electrochemical Science*[J], 2019, 14: 161
- 18 Huang J Y, Qiu Y B, Guo X P. *British Corrosion Journal*[J], 2013, 45(4): 288
- 19 Chen B A, Pan L, Wang R H et al. *Materials Science Engineering A*[J], 2011, 530: 607
- 20 Yu K, Li W, Li S et al. *Materials Science Engineering A*[J], 2004, 368(1-2): 88
- 21 Gazizov M, Teleshov V, Zakharov V et al. *Journal of Alloys Compounds*[J], 2011, 509(39): 9497
- 22 Lee S L, Wu C T, Chen Y T. *Journal of Materials Engineering Performance*[J], 2015, 24(5): 2170
- 23 Gong Z, Zheng Z Q, Jia M et al. *The Chinese Journal of Nonferrous Metals*[J], 2016, 26(6): 9 (in Chinese)
- 24 Fridlyander I N, Rokhlin L L, Dobatkina T V et al. *Metal Science Heat Treatment*[J], 1993, 35(10): 567
- 25 Li J F, Jia Z Q, Li C X et al. *Materials and Corrosion*[J], 2015, 60(6): 407
- 26 Ochs H, Vogelsang J. *Electrochimica Acta*[J], 2004, 49(17-18): 2973
- 27 Conde A, Damborenea J D. *Corrosion Science*[J], 2000, 42(8): 1363
- 28 Keddad M, Kuntz C, Takenouti H et al. *Electrochimica Acta*[J], 1997, 42(1): 87
- 29 Shi Y, Li M, Pan Q. *Journal of Alloys and Compounds*[J], 2014, 612: 42
- 30 Chen Y, Chen X, Liu T et al. *Journal of Chinese Society for Corrosion and Protection*[J], 2015(2): 7 (in Chinese)
- 31 Sheng H, Dong C F, Yang Z W et al. *Science & Technology Review*[J], 2012, 30(10): 6 (in Chinese)
- 32 Tao Z, Liu X, Shao Y et al. *Corrosion Science*[J], 2008, 50(12): 3500
- 33 Zhang J Q, Zhang Z, Wang J M et al. *Journal of Chinese Society for Corrosion and Protection*[J], 2001, 21(5): 11 (in Chinese)
- 34 Zhang J Q. *Electrochemical Measurement Technology*[M]. Beijing: Chemical Industry Press, 2010: 300 (in Chinese)
- 35 Yi Y N, Ma Y L, Luo X X et al. *Journal of Chongqing University of Technology (Natural Science)* [J], 2017, 31(4): 8 (in Chinese)

Sc添加对铸造Al-3Cu-1Li合金在酸性NaCl溶液中腐蚀行为的影响

鄂 顺¹, 邓佳诚², 王赫男¹, 冯长杰¹

(1. 沈阳航空航天大学 材料科学与工程学院, 辽宁 沈阳 110136)

(2. 新余钢铁集团有限公司, 江西 新余 338001)

摘要: 在 2 mol/L NaCl 酸性溶液中, 研究少量 Sc 对铸态 Al-3Cu-1Li 合金腐蚀行为的影响。通过 XRD 对铸态 Al-3Cu-1Li-xSc (质量分数) 合金进行相分析, 用 FE-SEM/EDS 和 TEM 观察了 Al-3Cu-1Li 合金和 Al-3Cu-1Li-0.5Sc 合金的显微组织; 采用极化曲线、电化学阻抗谱 (EIS)、电化学噪声 (EN) 和浸泡法对合金的腐蚀行为进行了研究, 并探讨腐蚀机制。结果表明: 含 Sc 的 Al-3Cu-1Li 合金晶内富 Cu 球形相减少, 晶界析出 W 相。随 Sc 含量的增加, 合金腐蚀反应的活化能降低, 阴极析氢速率增加, 自腐蚀电流密度增加, 合金的耐腐蚀性降低。添加 Sc 后, 合金在空气中形成的表面膜保护作用减弱至消失, 使含 Sc 合金的阻抗谱低频感抗弧逐渐消失。在 EN 测量期间, 不含 Sc 和含 0.1% Sc 的合金表面处于“膜破裂-再钝化”状态; 含 0.3% Sc 和 0.5% Sc 的合金发生严重的局部腐蚀 (晶间腐蚀), 且与 W 相有关。

关键词: Al-Cu-Li-xSc 合金; 酸性 NaCl 溶液; W 相; 富 Cu 相; 电化学噪声

作者简介: 鄂 顺, 男, 1996 年生, 硕士生, 沈阳航空航天大学材料科学与工程学院, 辽宁 沈阳 110136, E-mail: 1794500597@qq.com